

The Sunyaev-Zel’dovich effect and Faraday rotation contributions of galaxy groups to the CMB angular power spectrum

Hiroyuki Tashiro¹, Joseph Silk², Mathieu Langer¹ and Naoshi Sugiyama^{3,4}

¹ *Institut d’Astrophysique Spatiale (IAS), Bâtiment 121, F-91405, Orsay, France; Université Paris-Sud 11 and CNRS (UMR 8617)*

² *Astrophysics, Denys Wilkinson Building, The University of Oxford, Keble Road, Oxford OX1 3HR, UK*

³ *Department of Physics and Astrophysics, Nagoya University, Chikusa-ku, Nagoya, 464-8602, Japan*

⁴ *Institute for Physics and Mathematics of the Universe, University of Tokyo, 5-1-5 Kashiwa-no-Ha, Kashiwa, Chiba, 277-8582, Japan*

27 October 2018

ABSTRACT

The S-Z effect and Faraday rotation from halos are examined over a wide mass range, including gas condensation and magnetic field evolution. Contributions to the CMB angular power spectrum are evaluated for galaxy clusters, galaxy groups and galaxies. Smaller mass halos are found to play a more important role than massive halos for the B -mode polarisation associated with the S-Z CMB anisotropies. The B -modes from Faraday rotation dominate the secondary B -modes caused by gravitational lensing at $\ell > 3000$. Measurement of B -mode polarisation in combination with the S-Z power spectrum can potentially provide important constraints on intracluster magnetic field and gas evolution at early epochs.

Key words: cosmology: theory – magnetic fields – large-scale structure of the universe

1 INTRODUCTION

The baryonic components in galaxy clusters, galaxy groups and galaxies vary widely in their evolution. Some fraction of the baryons remains gaseous at the virial temperature and is threaded by microgauss magnetic fields, while a fraction condenses into the disk and forms stars. Therefore, knowing the temperature, density and the condensation rate of the baryons is an important clue for revealing the history of star formation, galaxy formation and even the magnetic field evolution and the reionisation process of the Universe.

The Sunyaev-Zel’dovich effect (S-Z effect) is an important tool for the investigation of baryon properties in halos (Sunyaev & Zeldovich 1972). The S-Z effect is the scattering of cosmic microwave background (CMB) photons by the hot electron gas in the gravitational potential wells of halos. As a result, the CMB frequency spectrum is distorted from the black-body spectrum. This distortion depends on the temperature and number density of the electron gas. In combination with X-ray observations, measuring the S-Z effect from galaxy clusters at each redshift gives the evolution of physical properties of the baryons (Morandi et al. 2007). Moreover, the temperature and the number density of the electron gas are related to the masses of halos, so that the number counts of detectable S-Z signals for different observational thresholds can provide the mass distribution of galaxy clusters. The distribution is sensitive to the cosmological parameters and to the non-Gaussianity of primordial density fluctuations. Therefore, the number counts of S-Z galaxy clusters can also give a constraint on the cosmological model (Bartelmann 2001; Moscardini et al. 2002; Schäfer et al. 2006; Sadeh et al. 2007). Many future CMB surveys

will make important contributions, and in some cases are even dedicated, to the measurement of S-Z-selected galaxy clusters (e.g. PLANCK¹, SPT², ACT³).

The S-Z effect from unresolved S-Z clusters is observed as CMB temperature anisotropies. These anisotropies are one of the major secondary anisotropies and dominant components for the high ℓ modes ($\ell > 2000$) in the angular temperature power spectrum. The amplitude strongly depends on the amplitude of matter density fluctuations, σ_8 . Small angular-scale CMB anisotropy experiments, BIMA (Dawson et al. 2002), CBI (Mason et al. 2003) and ACBAR (Kuo et al. 2007), have measured CMB anisotropies at high ℓ modes and detected the excess signal expected to be due to the S-Z effect. This excess corresponds to the S-Z effect with $\sigma_8 \sim 1.0$ (Bond et al. 2005; Douspis et al. 2006). However, this high value is in conflict with the 5 year WMAP result, $\sigma_8 \sim 0.8$, which is obtained from large-scale temperature anisotropies (Spergel et al. 2007). Note that this conflict is lifted when a possible contribution from unresolved point sources is taken into account (Douspis et al. 2006). In order to check whether the excess indeed is due to the effect of large σ_8 , we need detailed observational data on the S-Z number counts by future observations.

In this paper, we re-examine the number counts of S-Z halos and S-Z CMB anisotropies. Our aim is to clarify which halos with different masses contribute to any particular ℓ range. In particular, we focus on the S-Z effect of galaxy groups and galaxies ($M < 10^{14} M_\odot$). In those halos, the condensation of baryonic gas is effective. Clearly then, the S-Z effect is expected to depend on the evolution of gas condensation.

We also study Faraday rotation by magnetic fields in galaxy clusters, galaxy groups and galaxies. Many observations suggest that galaxy clusters and galaxies have magnetic fields whose amplitude is typically of the order of 1–10 μ Gauss. The coherence length of such magnetic fields can be as large as cluster virial scales, and structured magnetic fields have been found even on larger scales. (Kim et al. 1989). Besides, magnetic fields have been measured with the same amplitudes in high redshift objects at $z > 2$ (Athreya et al. 1998). However, the evolution of these fields has hitherto been unclear and is the one of the open questions in modern cosmology. In order to answer this question, we need statistical discussions of magnetic fields. In this paper, we discuss the potential of Faraday rotation as a probe of magnetic fields of galaxy clusters, galaxy groups and galactic halos by studying two observational methods. One is the number counts of Faraday rotation for S-Z halos. We calculate the number counts, and discuss the sensitivity of properties and evolution of magnetic fields in halo objects.

The other is the CMB B -mode polarisation observation. Faraday rotation distorts the CMB polarisation fields like gravitational lensing, so that it induces the B -mode polarisation from the E -mode. The angular power spectrum due to this effect in halos was studied by Takada et al. (2001) and Tashiro et al. (2008). In particular, Tashiro et al. (2008) pointed out that the angular power spectrum is sensitive to the magnetic field evolution and magnetic fields in galaxies can make a more dominant contribution than those in galaxy clusters. However, their adopted magnetic fields are simple toy models. Therefore, for a more detailed discussion, we study the CMB B -mode polarisation due to magnetic fields in halo objects based on observations and numerical simulations.

The paper is organised as follows. In Sec. II, we discuss the profiles of electron density and magnetic fields that we use, motivated by observations and numerical simulations. We calculate the number counts of halos for the S-Z effect and Faraday rotation in Sec. III. We discuss the impact of gas condensation and magnetic field evolution on the number counts. In Sec. IV, we compute the power spectrum of CMB temperature anisotropies by the S-Z effect and B -mode polarisation due to Faraday rotation. Sec. V is devoted to discussion and summary. Throughout the paper, we use the following cosmological parameters: $h = 0.7$ ($H_0 = h \times 100 \text{ km/s/Mpc}$), $T_0 = 2.725 \text{ K}$, $\Omega_B = 0.044$ and $\Omega_M = 0.27$ and $\sigma_8 = 0.8$.

2 HALO MODELS

2.1 Electron density and temperature profiles

For the electron density and temperature profiles in halos, we use the results of Komatsu & Seljak (2002), which are based on the NFW dark matter density profile (Navarro et al. 1997). The NFW dark matter density profile is given by

$$\rho_{\text{DM}}(x) = \frac{\rho_s}{x(1+x)^2}. \quad (1)$$

Here, $x \equiv r/r_s$ where r_s is a scale radius, and ρ_s is a scale density. The scale radius r_s is related to the virial radius by the concentration parameter c

$$r_s(M, z) = \frac{r_{\text{vir}}(M, z)}{c(M, z)}. \quad (2)$$

In the following, we adopt the concentration parameter of Komatsu & Seljak (2002) where

¹ <http://www.rssd.esa.int/index.php?project=Planck>

² <http://pole.uchicago.edu/>

³ <http://www.phy.princeton.edu/act>

$$c(M, z) \approx \frac{10}{1+z} \left[\frac{M}{M_*(0)} \right]^{-0.2}. \quad (3)$$

Here $M_*(0)$ is a solution to $\sigma(M) = \delta_c$ at the redshift $z = 0$ where σ is the variance smoothed with a top-hat filter of scale $R = (3M/4\pi\bar{\rho})^{1/3}$.

In order to obtain the profiles of the electron number density n_e and temperature T_e , Komatsu & Seljak (2002) considered three assumptions: (i) the electron gas is in hydrostatic equilibrium in the dark matter potential, (ii) the electron gas density follows the dark matter density in the outer parts of the halo, and (iii) the equation of state of the electron gas is polytropic, $P_e \propto \rho_e^\gamma$ where P_e , ρ_e and γ are the electron gas pressure, the gas density and the polytropic index, respectively. Under these assumptions, the electron number density and temperature profiles are simply given by

$$n_e = n_{ec} F(x), \quad (4)$$

$$T_e = T_{ec} F^{\gamma-1}(x). \quad (5)$$

Here, the dimensionless profile $F(x)$ is written as

$$F(x) = \left\{ 1 - A \left[1 - \frac{\ln(1+c)}{x} \right] \right\}^{1/(\gamma-1)}, \quad (6)$$

where the coefficient A is given by

$$A \equiv 3\eta_c^{-1} \frac{\gamma-1}{\gamma} \left[\frac{\ln(1+c)}{c} - \frac{1}{1+c} \right]^{-1}. \quad (7)$$

For γ and η_c , Komatsu & Seljak (2002) provided the following useful fitting formulae for γ and η_c ,

$$\gamma = 1.137 + 8.94 \times 10^{-2} \ln(c/5) - 3.68 \times 10^{-3} (c-5), \quad (8)$$

$$\eta_c = 2.235 + 0.202(c-5) - 1.16 \times 10^{-3} (c-5)^2. \quad (9)$$

The central electron density n_{ec} and the temperature T_{ec} are obtained as

$$n_{ec} = 3.01 \left(\frac{M}{10^{14} M_\odot} \right) \left(\frac{r_{\text{vir}}}{1 \text{ Mpc}} \right)^{-3} f_g \frac{c}{(1+c)^2} \left[\ln(1+c) - \frac{c}{1+c} \right]^{-1} \left[\frac{c}{c - F[c - \ln(1+c)]} \right]^{1/(\gamma-1)} \text{ cm}^{-3}, \quad (10)$$

$$T_{ec} = 0.88 \eta_c \left[\frac{M/(10^{14} h^{-1} M_\odot)}{r_{\text{vir}}/(1 h^{-1} \text{ Mpc})} \right] \text{ keV}, \quad (11)$$

where the gas fraction f_g represents the fraction of the gas that remains in the dark matter halo. The upper limit of this function is the background fraction of the baryon to the dark matter density $\Omega_B/\Omega_{\text{DM}}$.

Gonzalez et al. (2007) gave the fitting formula of the present day gas fraction as $\log f_{g0}(M) = -3.87 + 0.2 \log M$. In the early universe, gas condensation is not well advanced and the gas fraction can be assumed to be almost unity. As the universe evolves, gas condensation proceeds and star formation occurs in the condensed disk. Therefore, we assume that the evolution of the gas fraction is related to star formation by

$$f_g(z, M) = 1 - \frac{g(z)}{g(0)} [1 - f_{g0}(M)], \quad (12)$$

$$g(z) = \int^z dz' f_* dV/dz'. \quad (13)$$

Here, f_* is the star formation rate per comoving volume. We use the data in Bouwens et al. (2007) in order to obtain f_* . We show $f_g(z, M)$ in Fig. 1. The gas condensation starts around $z = 5$ in halos with mass lower than $10^{15} M_\odot$. However, in halos with mass larger than $10^{15} M_\odot$, the gas condensation is not effective and f_g almost equals the background ratio of baryonic to dark matter density $\Omega_B/\Omega_{\text{DM}}$.

2.2 Magnetic field distribution

The magnetic field profile in halos is not known in any detail. Observations by Murgia et al. (2004) suggest that the distribution of magnetic fields in galaxies and galaxy clusters is such that their strength decreases outwards. Accordingly, we consider two assumptions for magnetic fields in halos. The first one is that magnetic fields are frozen into the matter and therefore follow the gas density profile. The second is that the fields reach equipartition with thermal pressure in the central part in the halo. Under these assumptions, the present day magnetic field profile is written as

$$B(x) \propto B_c F^{2/3}(x), \quad (14)$$

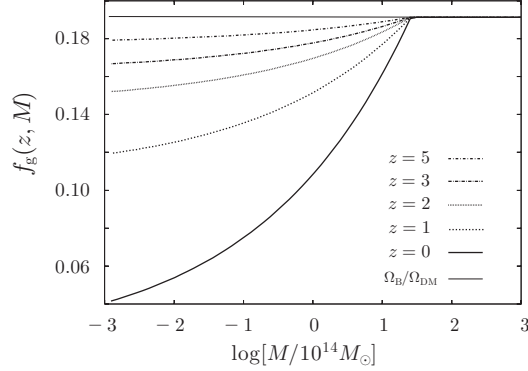


Figure 1. The gas fraction as a function of dark matter halo mass. The lines show the gas fractions in different redshifts: $z = 0$, $z = 1$, $z = 2$, $z = 3$ and $z = 5$ from bottom to top. For comparison, we plot Ω_B/Ω_{DM} as a thin line.

$$B_c = 2.0 \left(\frac{M}{10^{14} M_\odot} \right) \left(\frac{r_{\text{vir}}}{1 h^{-1} \text{Mpc}} \right)^{-2/3} \mu\text{Gauss}, \quad (15)$$

where B_c is the magnetic field strength at the centre of the halo with mass M , and is proportional to $M^{1/3}$.

The magnetic field evolution, especially in galaxy clusters, is unknown. Here, we adopt two cases for magnetic field evolution scenario. The first case is motivated by theoretical considerations, and the second case is based on numerical simulations.

CASE I

In the first case, we assume that the magnetic fields strength depends on the star formation rate via the evolution of the gas fraction. The magnetic field strength at redshift z is then given by

$$B(z) = \sqrt{\frac{g(z)}{g(0)}} B_0, \quad (16)$$

where B_0 is the magnetic field strength at present. This assumption is based on the theoretical idea that stars play an important role in the generation of magnetic fields. The seed magnetic fields are produced in stars and then spread over the halo by supernovae, AGN jets and galactic winds. They evolve rapidly over a dynamical time scale by the α - Ω dynamo in disks and small scale fluctuation dynamo in clusters (Brandenburg & Subramanian 2005). Finally, they reach micro-Gauss magnetic field strengths. In this case, the magnetic field strength is reduced to half of its present day value at $z \sim 3$.

CASE II

Case II is based on the numerical simulations of Dolag et al. (2002). They showed that the evolution of magnetic fields in galaxy clusters goes like $B(z) \propto e^{-2.5z}$. In this case we assume that the fields evolve as

$$B(z) = \begin{cases} e^{-2.5z} B_0, & M \geq M_*, \\ \sqrt{g(z)/g(0)} B_0, & M < M_*, \end{cases} \quad (17)$$

where M_* is the mass of the halo whose dynamical time scale equals the cooling time scale. In halos with mass smaller than M_* , the cooling time scale is shorter than the dynamical time scale. Therefore, such halos are expected to become star-forming galaxies. On the contrary, halos with mass larger than M_* , whose cooling time scales are larger than the dynamical time scale, end up as galaxy clusters or galaxy groups.

3 HALO NUMBER COUNTS

Galaxy clusters, galaxy groups and galaxies are good probes of the large scale structure of the Universe. For the S-Z effect, we can easily resolve a halo from the CMB sky map. The resolved number of halos for different masses and redshifts depends not only on the cosmology but also on the baryon physical properties. In particular, gas condensation has a serious effect on the number counts. In this section, we calculate the number counts, modeling gas condensation with a recipe based on recent observations. Moreover, we calculate the number counts for Faraday rotation. Faraday rotation in combination with S-Z effect is expected to provide a new constraint on magnetic fields in halos.

3.1 S-Z halo number counts

The change of the CMB intensity due to the S-Z effect can be written in terms of the Compton y -parameter as

$$\frac{\Delta I}{I_0} = Q(p)y, \quad (18)$$

where $p = h_p\nu/k_B T_{\text{CMB}}$ and $I_0 = (2h_p/c^2)(k_B T_{\text{CMB}})^3/h_p^3$ with the Boltzmann constant k_B and the Planck constant h_p . In Eq. (18), $Q(p)$ is given by

$$Q(p) = \frac{p^4 e^p}{(e^p - 1)^2} \left[\frac{p}{\tanh(p/2)} - 4 \right]. \quad (19)$$

The Compton y -parameter is given by

$$y = \int dl \frac{\sigma_T}{m_e} n_e k_B T_e, \quad (20)$$

where σ_T is the Thomson scattering cross section, and the integral is calculated along the line-of-sight in the cluster.

In order to discuss the S-Z signal from unresolved halo objects independently of frequency, it is convenient to define the quantity Y which is the value obtained by the integration of the y -parameter over the surface area of the halos,

$$Y = \frac{1}{D_A^2(z)} \int dA y(x), \quad (21)$$

where $D_A(z)$ is the angular diameter distance to the halo at redshift z and Y has a unit of a solid angle. For example, for the PLANCK satellite, the observable S-Z effect limit Y_{lim} corresponds to $3 \times 10^{-4} \text{arcmin}^2$ and can be derived from the optimal antenna temperature (Bartelmann 2001).

The temperature profile in halos, which is obtained in Sec. 2, is almost the isothermal profile. Therefore, it is valid to apply the isothermal assumption to Eq. (21) and we obtain

$$Y = \frac{f_g}{D_A^2(z)} \frac{1+X}{2} \frac{M}{m_p} \sigma_T \frac{kT_e}{m_e c^2}, \quad (22)$$

where X is the hydrogen ratio and is $X = 0.76$.

In order to calculate the number counts, we need to know the mass function of halos, $dn(M, z)/dM$. We adopt the fitting formula given by Sheth & Tormen (1999),

$$\frac{dn(M, z)}{dM} = \frac{\bar{\rho}}{M} \left(1 + 2^{-p} \frac{\Gamma(1/2 - p)}{\sqrt{\pi}} \right) (1 + (q\nu)^{-p}) \left(\frac{q\nu}{2\pi} \right)^{1/2} \exp\left(-\frac{q\nu}{2}\right) \frac{d\nu}{\nu}, \quad (23)$$

where $\nu = \left(\frac{\delta_c}{\sigma(M, z)} \right)^2$, δ_c is the critical over-density and σ is the variance smoothed with a top-hat filter of a scale $R = (3M/4\pi\bar{\rho})^{1/3}$ and we take $p = 0.3$, $q = 0.75$ (Cooray & Sheth 2002).

We plot the number counts of S-Z halos for a given Y_{lim} as a function of redshift in the left panel of Fig. 2. For comparison, we plot the number count distribution without gas condensation ($f_g = \Omega_B/\Omega_{\text{DM}}$ on all mass scales) as thin lines. This figure shows that most of the contribution comes from redshifts lower than 0.5. The difference between the cases with and without gas condensation becomes a little bit larger at low redshifts than at high redshifts. We find that the peak position of the number count does not depend on gas condensation, and the number count in the case with gas condensation at redshifts lower than 0.5 is about half of that without gas condensation.

The right panel in Fig. 2 shows the number counts of S-Z halos for a given Y_{lim} as a function of mass. In the spherical model, the electron temperature for given mass and redshift is proportional to $M^{2/3}(1+z)$. Since halos with larger masses produce stronger signals, they are easy to detect. Therefore, the number counts on the right side of the peak do not depend on Y_{lim} and are determined only by the mass function of halos. This is why all plots for different Y_{lim} lie on the same line.

The electron temperature is proportional to $z+1$. Besides, the angular diameter distance increases until about $z \sim 2$, and declines for higher redshifts. Accordingly, the S-Z signal Y reaches a minimum around $z \sim 1$. At this redshift, the signal becomes lower than Y_{lim} for halos whose mass is smaller than a certain corresponding mass M_{lim} . The peak position is determined by this mass, and its position depends strongly on the gas fraction. The sharpness of the peak strongly depends on the derivative of the mass function at Y_{lim} . For high Y_{lim} , M_{lim} is large so that the slope of mass function at this mass scale is steep. On the contrary, a lower Y_{lim} corresponds to a smaller M_{lim} where the mass function is almost flat.

The gas condensation has an effect on the number counts on small mass scales. The smaller the halo mass, the larger is the deviation between the cases with and without gas condensation. This is because gas condensation is important for the small mass halos as shown in Fig. 1.

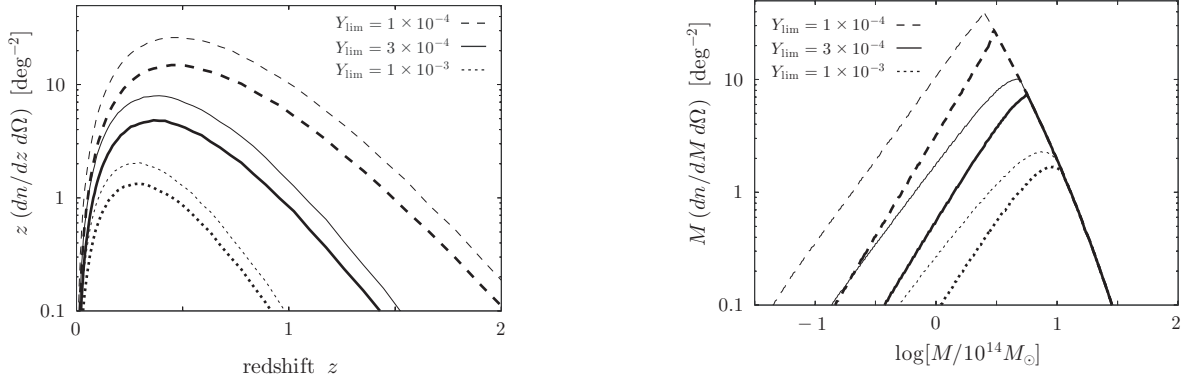


Figure 2. The number counts of S-Z halos. In both panels, the dashed, solid and dotted lines represent the number counts for $Y_{\text{ion}} = 1.0 \times 10^{-4}$, 3.0×10^{-4} and 1.0×10^{-3} , respectively. For comparison, we put the number counts without gas condensation as thin lines. In the left panel, we show the number counts of S-Z halos as a function of redshift. In the right panel, we plot the number counts of S-Z halos as a function of halo mass.

3.2 Faraday rotation measurements

Next, we investigate Faraday rotation in the S-Z halos. The change of the polarised rotation angle by Faraday rotation is written as

$$\alpha = \lambda^2 RM. \quad (24)$$

Here, λ is the wave-length and RM is the rotation measure, which characterises the Faraday rotation, given by

$$RM = \frac{e^3}{2\pi m_e^2} \int dl n_e B \hat{\gamma} \cdot \hat{b}. \quad (25)$$

where B is the magnetic field strength along the line of sight, and $\hat{\gamma}$ and \hat{b} are the orientations of the line of sight and magnetic fields.

We calculate the rotation measure along the path that intersects the centre of the S-Z halos. For simplicity, we also assume that the coherence length of magnetic field is the virial radius and that the orientations are random. This assumption yields $\langle |\hat{\gamma} \cdot \hat{b}|^2 \rangle = 1/3$.

We plot the number distribution of the rotation measure as a function of the redshift in the left panel of Fig. 3. We have set $Y_{\text{ion}} = 3 \times 10^{-4}$ and we show the number counts for case I and case II of the magnetic field evolution. As we increase the threshold of the rotation measurement, we fail to detect small mass halos, because the rotation measurement strongly depends on the halo mass. This failure accounts for the lack of detectable numbers of halos in low redshifts. In case I, the magnetic field evolution is very slow, so that the halos with large mass, even at high redshifts, produce a large rotation measurement. Since S-Z halos at high redshifts have large masses, we can detect all of them in case I. On the other hand, case II has rapid magnetic field evolution at low redshift. Therefore, since the amplitude of magnetic fields becomes very small at high redshifts, we cannot detect the signal from high redshift halos. As a result, the distribution of the number counts over redshift in case II is suppressed.

The right panel in Fig 3 shows the number count distribution as a function of mass. As in Fig. 3, we have set $Y_{\text{ion}} = 3 \times 10^{-4}$ and we plot the number counts for case I and case II of magnetic field evolution. The threshold determines the detectable minimum mass of S-Z halos at each redshift. Although the minimum mass at present does not depend on the evolution of magnetic fields, as the redshift increases, a difference arises between cases I and II. In case II where the evolution is rapid, since even large mass halos cannot produce rotation measures above the threshold, we can detect fewer halos than in case I. However, halos with sufficiently large masses, even at high redshift, can produce larger rotation measures. The peak of the number counts is located at this critical minimum mass and all S-Z halos with larger masses are detectable. The peak position is sensitive to the threshold and the evolution of magnetic fields. This implies that varying the threshold of the rotation measurement can give us the number counts of S-Z halos with the corresponding mass scale and a constraint on magnetic field evolution.

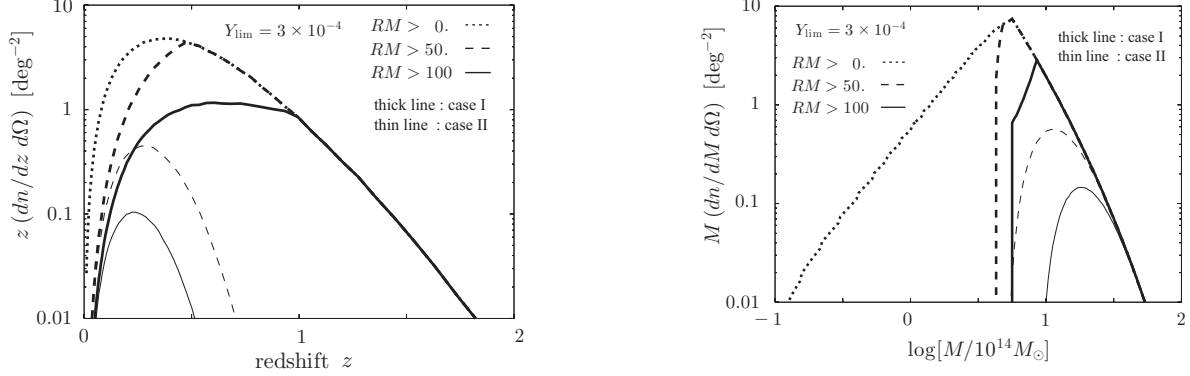


Figure 3. The number counts of S-Z halos with $Y_{\text{lim}} = 3.0 \times 10^{-4}$ for rotation measurements. In both panels, the number counts for $RM > 0$, $RM > 50$ and $RM > 100$ are plotted as dotted, dashed and solid lines, respectively. The thick lines are for case I and the thin lines are for case II. In the left panel, we give the number counts as a function of redshift. In the right panel we plot the number counts as a function of halo mass.

4 CMB ANISOTROPIES DUE TO S-Z EFFECT AND FARADAY ROTATION

4.1 Angular power spectrum of S-Z effect and Faraday rotation

Halos with S-Z signals lower than Y_{lim} contribute to the diffuse temperature anisotropies and cannot be individually removed from the CMB map. The computation of the angular power spectrum of S-Z temperature anisotropies is based on the halo formalism (Cole & Kaiser 1988; Makino & Suto 1993; Komatsu & Kitayama 1999),

$$C_\ell^{SZ} = g_\nu^2 \int_0^{z_{\text{max}}} dz \frac{dV}{dz} \int_{M_{\text{min}}}^{M_{\text{max}}} dM \frac{dn(M, z)}{dM} |y_\ell(M, z)|^2, \quad (26)$$

where g_ν is the spectral function of the S-Z effect, which is -2 in the Rayleigh-Jeans limit. In Eq. (26), $y_\ell(M, z)$ is the 2D Fourier transform of the projected Compton y -parameter and is obtained from

$$y_\ell = \frac{4\pi r_s}{\ell_s^2} \int_0^\infty dx x^2 y_{3d}(x) \frac{\sin(\ell x / \ell_s)}{\ell x / \ell_s}, \quad (27)$$

where y_{3d} is the radial profile of Compton y -parameter,

$$y_{3d}(x) = \frac{\sigma_T}{m_e} n_e(x) k_B T_e(x), \quad (28)$$

and ℓ_s is the angular wavenumber corresponding to r_s , $\ell_s = D_A / r_s$.

Faraday rotation in halos produces the secondary B -mode polarisation from primary E -mode polarisation. The produced B -mode angular power spectrum is given by (Takada et al. 2001; Tashiro et al. 2008)

$$C_\ell^{\text{Fara}} = N_\ell^2 \sum_{\ell_1 \ell_2} N_{\ell_2}^2 K(\ell, \ell_1, \ell_2)^2 C_{\ell_2}^E C_{\ell_1}^\alpha \frac{(2\ell_1 + 1)(2\ell_2 + 1)}{4\pi(2\ell + 1)} (C_{\ell_1 0 \ell_2 0}^{\ell_0})^2, \quad (29)$$

where $C_{\alpha\beta\gamma}^{\alpha\beta\gamma}$ are the Clebsch-Gordan coefficients, $N_\ell = (2(\ell - 2)! / (\ell + 2)!)^{1/2}$ and

$$K(\ell, \ell_1, \ell_2) \equiv -\frac{1}{2} (L^2 + L_1^2 + L_2^2 - 2L_1 L_2 - 2L_1 L - 2L_2 - 2L), \quad (30)$$

with $L = \ell(\ell + 1)$, $L_1 = \ell_1(\ell_1 + 1)$, and $L_2 = \ell_2(\ell_2 + 1)$. In Eq. (29), C_ℓ^E is the primary E -mode polarisation angular spectrum and C_ℓ^α is the angular power spectrum of the rotation measurements. The expression of C_ℓ^α is

$$C_\ell^\alpha = \int_0^{z_{\text{dec}}} dz \frac{dV}{dz} \int_{M_{\text{min}}}^{M_{\text{max}}} dM \frac{dn(M, z)}{dM} |\alpha_\ell(M, z)|^2, \quad (31)$$

where $\alpha_\ell(M, z)$ is the projected Fourier transform of the rotation angle obtained in the small angle approximation,

$$\alpha_\ell = 2\pi \int d\theta \theta \alpha(\theta, M, z) J_0(\ell\theta). \quad (32)$$

Here $\alpha(\theta, M, z)$ is the angular profile of the rotation measurement induced by magnetic fields in a halo with mass M at redshift z and θ is the angular separation from the centre of a halo.

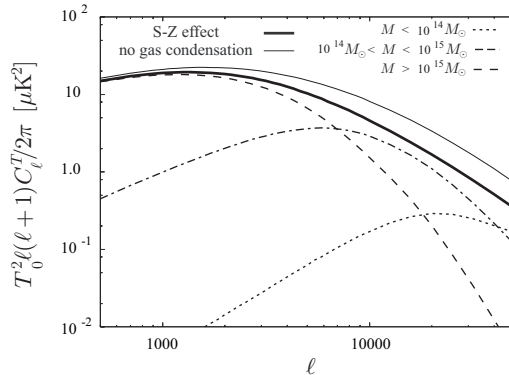


Figure 4. Angular power spectra of the S-Z effect. The contributions from collapsed halo objects with $M < 10^{14} M_\odot$, $10^{14} M_\odot < M < 10^{15} M_\odot$ and $M > 10^{15} M_\odot$ are represented as dotted, dotted-dashed, dashed lines, respectively. For comparison, we plot the spectrum of the S-Z effect without gas condensation.

4.2 Results

First, we plot the S-Z angular power spectrum in Fig. 4. Around the peak, the main contribution comes from massive halos ($M > 10^{15} M_\odot$). However, halos with masses smaller than $10^{15} M_\odot$ become important in the high ℓ modes. The contribution from halos with masses $10^{14} M_\odot < M < 10^{15} M_\odot$ and with masses $M < 10^{14} M_\odot$ dominate at $\ell \sim 10000$ and $\ell > 50000$, respectively. For comparison, we plot the spectrum of the S-Z effect without gas condensation as a thin line. The smaller the halos are, the more efficient gas condensation becomes. Therefore, the difference between the spectra with and without gas condensation is large for the high ℓ modes.

Next, we show the angular power spectrum of Faraday rotation measurements in Fig. 5. In this figure, we set the CMB frequency to 30 GHz. The position of the peak is around $\ell = 5000$ or $\ell = 10000$, depending on the magnetic field evolution. This peak position is on higher ℓ than for the S-Z power spectrum and the main contribution around the peak is produced by halos with $10^{14} M_\odot < M < 10^{15} M_\odot$. Compared with the S-Z effect, halos with small masses are more important in rotation measurements. The mass dependence of the S-Z effect is $y \sim n_e T_e R \propto M$, while that of rotation measurements is $RM \sim n_e B R \propto M^{2/3}$. This fact makes the scale where the S-Z contribution from halos with small masses dominate shift to low ℓ modes. For rotation measurements, halos with $M > 10^{15} M_\odot$ dominate around $\ell \sim 1000$ and halos with mass $10^{14} M_\odot < M < 10^{15} M_\odot$ and with mass $M < 10^{14} M_\odot$ overwhelm other components at $\ell \sim 6000$ and $\ell > 20000$, respectively. In the left panel of Fig. 5, we show the dependence on the magnetic field evolution. Rapid evolution as in case II suppresses the amplitude at high ℓ modes ($\ell > 2000$), because these are produced by halos around $z \sim 0.5$ where the magnetic field energy becomes half of its present-day value (see also Fig. 6 in Tashiro et al. 2008).

The angular power spectra of CMB B -mode polarisation induced by Faraday rotation is shown in Fig. 6. These power spectra reflect the angular power spectra of the rotation measurements. The effect of small halos arises at lower ℓ modes than for the S-Z effect. Although the contribution from halos with $M < 10^{15} M_\odot$ is sub-dominant for the S-Z power spectrum, these still provide a major contribution to the Faraday B -mode spectrum. Halos with $10^{14} M_\odot < M < 10^{15} M_\odot$ dominate over halos with larger masses for $\ell > 2000$. This should have important observational implications. On scales where the contributions of halos with $M > 10^{15} M_\odot$ are dominant, the B -modes from Faraday rotation are overwhelmed by the B -modes from gravitational lensing. The detection of the B -modes from Faraday rotation is expected for ℓ modes bigger than $\ell = 3000$. The gas and magnetic field properties of galaxy groups and galaxies are important for the B -modes produced by Faraday rotation.

Regarding magnetic field evolution, as shown in the left panel of Fig. 6, an effect is apparent on small scales. Rapid magnetic field evolution as in case II strongly suppresses the amplitude of high ℓ modes. This is also related to the decrease of the Faraday rotation in small mass halos. We conclude that the measurement of B -mode Faraday rotation can put constraints on gas and magnetic field evolution.

5 CONCLUSION

In this paper, we examine the S-Z effect and Faraday rotation from halos which have a wide mass range ($10^{12} M_\odot < M < 10^{17} M_\odot$). In particular, we take into account the effects of gas cooling based on recent observations and consider two cases for magnetic field evolution motivated by theoretical considerations and numerical simulations.

First, we calculate the halo number counts for the S-Z effect. We find that the number counts for the S-Z effect are sensitive to gas condensation. The redshift distribution is suppressed by gas condensation over all redshifts. In the mass distribution,

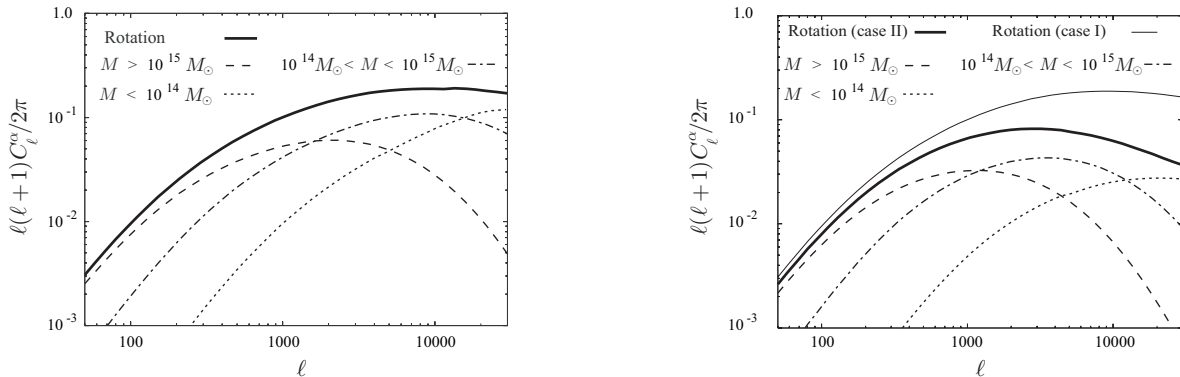


Figure 5. Angular power spectra of rotation measurements. The contributions from halos with $M < 10^{14} M_\odot$, $10^{14} M_\odot < M < 10^{15} M_\odot$ and $M > 10^{15} M_\odot$ are given as the dotted, dotted-dashed, dashed lines, respectively. We set the CMB frequency to 30 GHz. In the left panel, we plot the angular power spectra in case I. In the right panel, we show the spectra in case II. For comparison, we plot the spectrum in case I as a thin solid line.

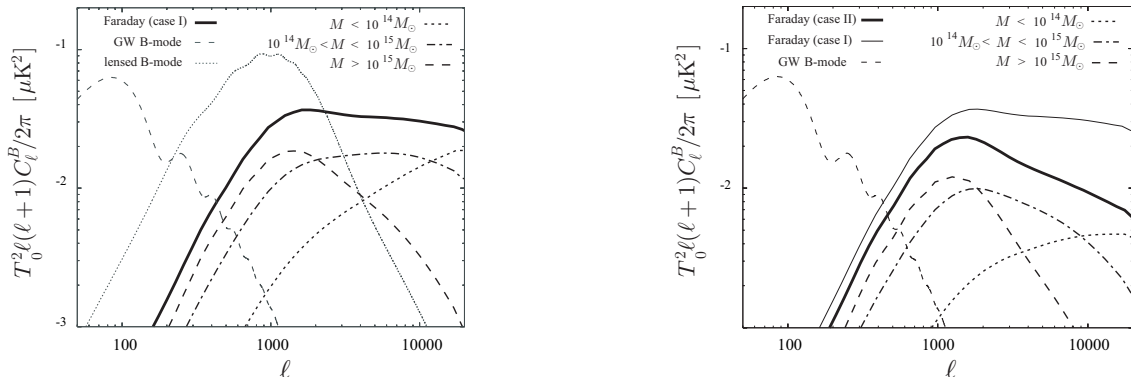


Figure 6. Angular power spectra of CMB B -mode polarisation produced by Faraday rotation. In both panels, the dotted, dotted-dashed, dashed lines represent the contributions from halos with $M < 10^{14} M_\odot$, $10^{14} M_\odot < M < 10^{15} M_\odot$ and $M > 10^{15} M_\odot$, respectively. We set the CMB frequency to 30 GHz. In the left panel, we plot the B -mode angular power spectra in case I of the magnetic field evolution. For comparison, we put the GW B -mode and lensed B -mode as the thin dashed and thin dotted lines, respectively. In the right panel, we show the spectra in case II. For comparison, we give the B -mode spectrum in case I as the thin solid line.

gas condensation suppresses the number counts on small scales. As a result, the peak position of the distributions shifts to larger mass scales.

We also calculate the rotation measurement for S-Z halos. The distribution of number counts strongly depends on the magnetic field evolution. The detectable minimum mass is decided by the threshold of rotation measure. Therefore, by varying the threshold we can obtain number counts of S-Z halos over the corresponding mass scales and constrain the magnetic field evolution.

We study the CMB angular power spectrum arising from the S-Z effect and Faraday rotation in galaxy clusters, galaxy groups and galactic halos. For the S-Z effect, the main contribution comes from massive halos ($M > 10^{15} M_\odot$). These set the peak at around $\ell \sim 2000$. Halos with mass $M < 10^{14} M_\odot$ dominate the contribution on small scales. The S-Z effect in halos with mass $10^{14} M_\odot < M < 10^{15} M_\odot$ and with mass $M < 10^{14} M_\odot$ produces CMB anisotropies over $\ell \sim 10000$ and $\ell > 50000$, respectively. Gas condensation is effective on small mass scales so that it suppresses the CMB anisotropies at $\ell \sim 10000$.

For the B -mode polarisation, small mass halos play more important roles than for the S-Z CMB anisotropies. As a result, the B -modes produced in such small halos arise on larger ℓ scales than the S-Z CMB anisotropies. The peak of the B -mode power spectrum is produced by halos with $10^{14} M_\odot < M < 10^{15} M_\odot$ and is located at $1000 < \ell < 5000$. Halos with $M > 10^{15} M_\odot$ are dominant around $\ell \sim 1000$ and B -modes produced by halos with mass $M < 10^{14} M_\odot$ arise at $\ell > 20000$, respectively. The evolution of magnetic fields modifies the amplitude produced by halos with $M < 10^{14} M_\odot$. The small mass halos at high redshift can collectively generate detectable B -mode polarisation. However, since the halos at high redshift are easily affected by the evolution of magnetic fields, the B -modes by such halos are rapidly damped in the rapid evolution case.

Comparing to other B -mode polarisation contributions, the B -modes from Faraday rotation dominate the secondary B -modes caused by gravitational lensing at $\ell < 3000$. On these scales, the B -modes by Faraday rotation are produced by halos with mass $M < 10^{14} M_\odot$. Therefore, measurement of such B -mode polarisation could put constraints on magnetic field evolution, in combination with the S-Z power spectrum.

ACKNOWLEDGEMENTS

NS is supported by a Grant-in-Aid for Scientific Research from the Japanese Ministry of Education (No. 17540276).

REFERENCES

- Athreya R. M., Kapahi V. K., McCarthy P. J., van Breugel W., 1998, *A&A*, 329, 809
Bartelmann M., 2001, *A&A*, 370, 754
Bond J. R. et al., 2005, *ApJ*, 626, 12
Bouwens R. J., Illingworth G. D., Franx M., Ford H., 2007, *ApJ*, 670, 928
Brandenburg, A. and Subramanian, K., 2005, *Phys. Rep.*, 417, 1
Cole S., Kaiser N., 1988, *MNRAS*, 233, 637
Cooray A., Sheth R., 2002, *Phys.Rep.*, 372, 1
Dawson K. S., Holzapfel W. L., Carlstrom J. E., Joy M., LaRoque S. J., Miller A. D., Nagai D., 2002, *ApJ*, 581, 86
Dolag K., Bartelmann M., Lesch H., 2002, *A&A*, 387, 383
Douspis, M., Aghanim, N. and Langer, M., 2006, *A&A*, 456, 819
Gonzalez A. H., Zaritsky D., Zabludoff A. I., 2007, *ApJ*, 666, 147
Kim K.-T., Kronberg P. P., Giovannini G., Venturi T., 1989, *Nature*, 341, 720
Komatsu E., Kitayama T., 1999, *ApJ*, 526, L1
Komatsu E., Seljak U., 2002, *MNRAS*, 336, 1256
Kosowsky A., Kahniashvili T., Lavrelashvili G., Ratra B., 2005, *Phys. Rev. D*, 71, 043006
Kuo C. L. et al., 2007, *ApJ*, 664, 687
Makino N., Suto Y., 1993, *ApJ*, 405, 1
Mason B. S. et al., 2003, *ApJ*, 591, 540
Morandi A., Etti S., Moscardini L., 2007, *MNRAS*, 379, 518
Moscardini L., Bartelmann M., Matarrese S., Andreani P., 2002, *MNRAS*, 335, 984
Murgia M., Govoni F., Feretti L., Giovannini G., Dallacasa D., Fanti R., Taylor G. B., Dolag K., 2004, *A&A*, 424, 429
Navarro J. F., Frenk C. S., White S. D. M., 1997, *ApJ*, 490, 493
Sadeh S., Rephaeli Y., Silk J., 2007, *MNRAS*, 380, 637
Schäfer B. M., Pfrommer C., Bartelmann M., Springel V., Hernquist L., 2006, *MNRAS*, 370, 1309
Sheth R. K., Tormen G., 1999, *MNRAS*, 308, 119
Spergel D. N. et al. 2007, *ApJS*, 170, 377
Sunyaev R. A., Zel'dovich Y. B., 1972, *Comments on Astrophysics and Space Physics*, 4, 173
Takada M., Ohno H., Sugiyama N., 2001, *astro-ph/0112412*
Tashiro H., Aghanim N., Langer M., 2008, *MNRAS*, 384, 733